Univerzita Karlova v Praze

Matematicko-fyzikální fakulta

DIPLOMOVÁ PRÁCE

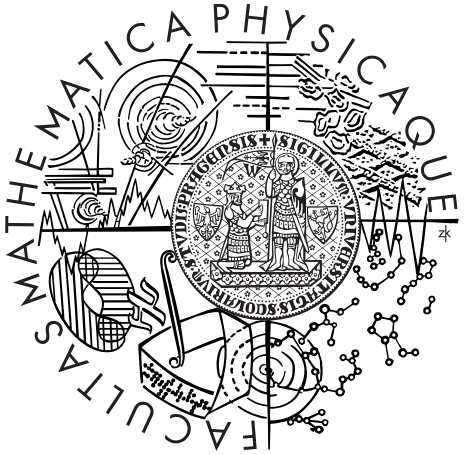

Pavel Malý

Jednomolekulární spektroskopie fotosyntetických antenních systémů

Fyzikální ústav Univerzity Karlovy

Vedoucí diplomové práce: RNDr. Tomáš Mančal, Ph.D.
Studijní program: Fyzika
Specializace: Optika a optoelektronika

Praha 2014

Charles University in Prague

Faculty of Mathematics and Physics

MASTER THESIS

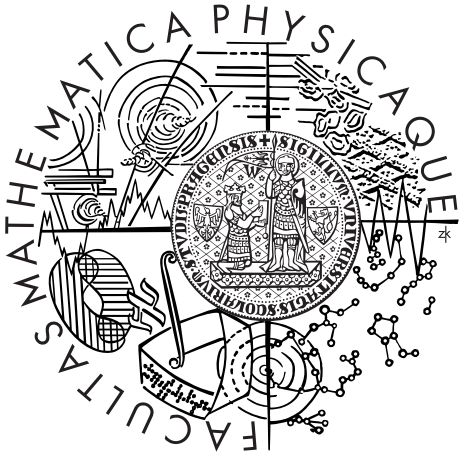

Pavel Malý

Single-molecule spectroscopy of photosynthetic antenna systems

Institute of Physics of Charles University in Prague

Supervisor of the master thesis: RNDr. Tomáš Mančal, Ph.D.
Study programme: Physics
Specialization: Optics and optoelectronics

Prague 2014

I would like to thank my supervisor Tomáš Mančal for his support, encouragement and trust. I would also like to thank Rienk van Grondelle for the most friendly welcome in his group in Amsterdam. And, finally, my thanks belong to Michael Gruber, who showed me the single-molecule setup and always had time for interesting discussions.

I declare that I carried out this master thesis independently, and only with the cited sources, literature and other professional sources.

I understand that my work relates to the rights and obligations under the Act No. 121/2000 Coll., the Copyright Act, as amended, in particular the fact that the Charles University in Prague has the right to conclude a license agreement on the use of this work as a school work pursuant to Section 60 paragraph 1 of the Copyright Act.

In ..... date ..... signature of the author

Název práce: Jednomolekulární spektroskopie fotosyntetických antenních systémů

Autor: Pavel Malý

Katedra: Fyzikální ústav Univerzity Karlovy

Vedoucí diplomové práce: RNDr. Tomáš Mančal, Ph.D., Fyzikální ústav Univerzity Karlovy

Abstrakt: V posledních letech odhalily experimenty jednomolekulární spektroskopie (SMS) mnoho zajímavých statických i dynamických vlastností fotosyntetických komplexů. Součástí této práce jsou jednomolekulární experimenty na monomerech LHCII, kde jsou pozorovány všechny efekty, které byly dříve popsány na trimerech LHCII. Zatímco jednotlivě byly některé tyto výsledky vysvětleny různými modely, kvůli širokému rozsahu důležitých časových škál od ps do minut nebyl zatím učiněn pokus simulovat tyto experimenty v rámci jednoho modelu. V této práci jsou odvozeny aproximované rovnice založené na excitonovém modelu, které popisují dynamiku systému na všech časových škálách důležitých pro SMS. Platnost těchto rovnic je demonstrována simulací souborových a jednomolekulárních spekter monomerů LHCII. Na základě našeho modelu je ukázáno, že Lut 1 může efektivně zhášet fluorescenci LHCII. S použitím konformační změny LHCII proteinu jako přepínacího mechanismu jsou simulovány intenzitní a spektrální časové stopy jednotlivých komplexů a experimentální statistická rozdělení jsou reprodukována.

Klíčová slova: Jednomolekulární spektroskopie, LHCII, blikání, NPQ

Title: Single-molecule spectroscopy of photosynthetic antenna systems

Author: Pavel Malý

Department: Institute of physics of the Charles University

Supervisor: RNDr. Tomáš Mančal, Ph.D., Institute of physics of the Charles University

Abstract: In recent years Single-Molecule Spectroscopy (SMS) experiments revealed many interesting static and dynamic properties of photosynthetic complexes. In this thesis single-molecule experiments on LHCII monomers are performed and all the effects described previously on LHCII trimers are observed. While separately some of the results have been explained by various models, because of broad range of important timescales from ps to minutes no attempt to simulate these experiments within one model was made. In this thesis approximated equations based on the excitonic model are derived, describing the system dynamics on all timescales important for SMS. Validity of these equations is demonstrated by simulating ensemble and single-molecule spectra of LHCII monomers. Based on our model it is shown that Lut 1 can act as an efficient fluorescence quencher in LHCII. Using conformational change of the LHCII protein as a switching mechanism the intensity and spectral time traces of individual complexes are simulated and the experimental statistical distributions are reproduced.

Keywords: Single-molecule spectroscopy, LHCII, blinking, NPQ

Contents

Introduction

In the last decades of 20th century the experimental techniques advanced so far that it became possible to observe and manipulate individual molecules and molecular structures. One of several possible techniques is optical excitation of individual molecules and detection of their subsequent fluorescence. Because this type of spectroscopy contains significantly more information than traditional ensemble spectroscopic measurements, it brings, together with more knowledge, also some new challenges for interpretation and theoretical explanation. Typical example of a completely new phenomenon exhibited by almost all single fluorescing objects, i.e. molecules, nanocrystals etc., is fluorescence intermittency[1]. In the ensemble measurement this completely averages out, because the molecules are not synchronized. But when looking at a single object fluorescence, it is often found that it blinks. What is more, the blinking statistics are very similar for very different systems and they typically span broad range of timescales. This phenomenon was also observed on individual photosynthetic antenna complexes. As their role *in vivo* is light absorption and subsequent energy transfer, interesting questions arise about the influence of the dynamical change of their spectroscopic properties on their antenna function. For instance, there are intriguing possibilities in connecting the above mentioned blinking to the light harvesting regulation, the mechanism of which is a long-debated and still not fully solved issue. Finally, as the accessible timescale is in the range of milliseconds to minutes, which corresponds to protein dynamics, the single-molecule experiments could provide significant insight into the role of the protein dynamics in light harvesting.

Because the pigment-protein complexes are much more prone to being damaged by unstable environment or high illumination intensity, their observation on the single-complex level presents a more serious experimental challenge than, for example, quantum dots. That is why the single-molecule spectroscopy (SMS) experiments on several photosynthetic antenna complexes including major light harvesting complex II (LHCII) of higher plants were performed only recently [10, 25]. The results of such measurements include fluorescence spectral peak distributions, spectral diffusion, fluorescence intensity distributions and time traces. In the case of LHCII many interesting effects have been observed such as the fluorescence intermittency and also spectral diffusion including small drifting or rapid shifting of the fluorescence peak position and appearance of a second peak. It has been conjectured that the blinking could be connected to regulated energy dissipation, i. e. non-photochemical quenching (NPQ) [11].

LHCII naturally occurs in the trimeric form, i. e. consisting of three identical subunits [13]. The first goal of the work contained in this thesis was to measure the single-molecule signals of these LHCII monomeric subunits to find out whether they also exhibit the above mentioned phenomena. It turns out that they do, which means they can be treated as the smallest functional subunit and in the theoretical description it is enough to start with only one monomer.

As far as the theory is concerned, the ensemble-averaged spectra and also the spectral peak distributions can be very successfully explained by the disordered excitonic model, as was demonstrated by Novoderezhkin and coworkers [12]. As we will see further on, the excitonic model usually operates on fs to ps timescale. On the timescale of the typical single-molecule measurement it thus describes the 'static' properties without providing a dynamic information such as amount of spectral diffusion on ms scale.

The switching between the fluorescent and dark state can be modelled by a 2-level switching model developed by Valkunas and coworkers [31]. This model is purely phenomenological and has no relation to the excitonic model, i. e. to the actual system dynamics. As this model describes the fluorescence blinking, it operates on ms to min timescale.

Because of this large timescale mismatch and lack of mechanism connecting the excitonic and switching model, no theoretical attempt was made so far to model the actual system dynamics on the timescale of the single-molecule experiments within one model. In this thesis such an attempt is made. From the equations of the excitonic model approximate equations for excitonic populations are derived, which hold for long times. This allows the connection with the switching model by slowly changing the parameters of the excitonic model. This results in modelling the outcome of the single-molecule experiment both regarding the "statical" information as spectral distributions and "dynamical" information such as time-resolved intensity and spectral traces. Although the results are demonstrated on LHCII monomers, the developed theory is more general and can be used on any single-molecule measurement on a system to which the employed approximations apply.

Finally, the way how and which parameters should be changed by the switching depends on the particular system of interest and remains to be determined. To that purpose we employ a NPQ mechanism proposed by Ruban [26], the energy transfer to carotenoid lutein on which the excitation quickly relaxes. This allows us to connect our model to the NPQ picture, one step further to forming a consistent description of LHCII in the framework of its biological role.

The thesis is structured as follows. In the first chapter a brief introduction to SMS is given, the experimental setup on which the results were measured is described together with the kinds of experimental signals obtained. Also the sample preparation and data analysis are briefly described.

In the first part of Chapter 2 the excitonic model of molecular systems as open quantum systems is introduced. The second part of this chapter presents our derivation of equations for the excitonic populations, which are valid in broad time scale ranging from 10 ps to 10 s and which therefore provide good theoretical basis for the single-molecule time-resolved experiments description.

In Chapter 3 the protein conformation switching model is introduced. The original description by continuous-time probability density evolution is presented and the modification for discrete random walk allowing for following individual single complexes is derived. The differences between our model and the original model by Valkunas [31] are also mentioned and justified.

In Chapter 4 the theory is applied on LHCII. After a brief description of LHCII, its role in photosynthesis and structure, the excitonic model is constructed and the absorption and fluorescence spectrum is modelled. Afterwards the energy transfer to Lutein 1 is included as a fluorescence quenching mechanism and the parameters of the lutein are investigated. It is shown that for parameters consistent with previous research work the lutein can act as an efficient fluorescence quencher. Then the parameters of the protein switching model are adjusted to fit the on/off dwell time distributions, which makes the model ready for use in controlling the excitonic model. Finally, the results from the previous sections are connected and the switching model is used to change the coupling to Lut 1, which results in controlling the fluorescence given by the excitonic model. This enables us to simulate the intensity and spectral time traces. The obtained statistics are compared to the experimental results and the agreement is shown and commented on.

1. Single molecule spectroscopy

1.1 Overview

To this date there are several different methods available which can observe/manipulate single molecules/complexes, including single-molecule fluorescence. The advantages of this approach are its less perturbative nature compared to contact methods and better signal-to-background ratio compared to single molecule absorption measurement. The disadvantage is lower, diffraction-limited spatial resolution and relatively weak fluorescence signal. The former is solved by low molecule concentration, resulting in only one molecule in an excitation volume. The latter can be to some extent improved by using confocal imaging, as was the case in this work, but extraction of the signal still remains the most serious experimental challenge and thus becomes the limiting factor determining the time and spectral resolution of the measurement. The weak signal problem is even more pronounced in biological samples such as those considered in this thesis, since high illumination power can lead to irreversible photobleaching and damage of the molecule.

Although the realization is complex, the obtained results more than justify the effort, as much more information compared to ensemble measurement is obtained. First, instead of average values for the observables such as spectrum, intensity etc. the whole distribution is obtained. Second, rare realizations, which are in ensemble measurement completely hidden, can be observed. And finally, new phenomena such as fluorescence intermittency and spectral diffusion can appear, while in traditional measurement only the mean value can be observed. As we will see in section 4.2 examples of all of the points mentioned above have been observed in LHCII.

1.2 Experimental setup

Fig. 1.1 taken from Ref. [10] depicts an experimental setup in LaserLab at VU Amsterdam used for the measurements.

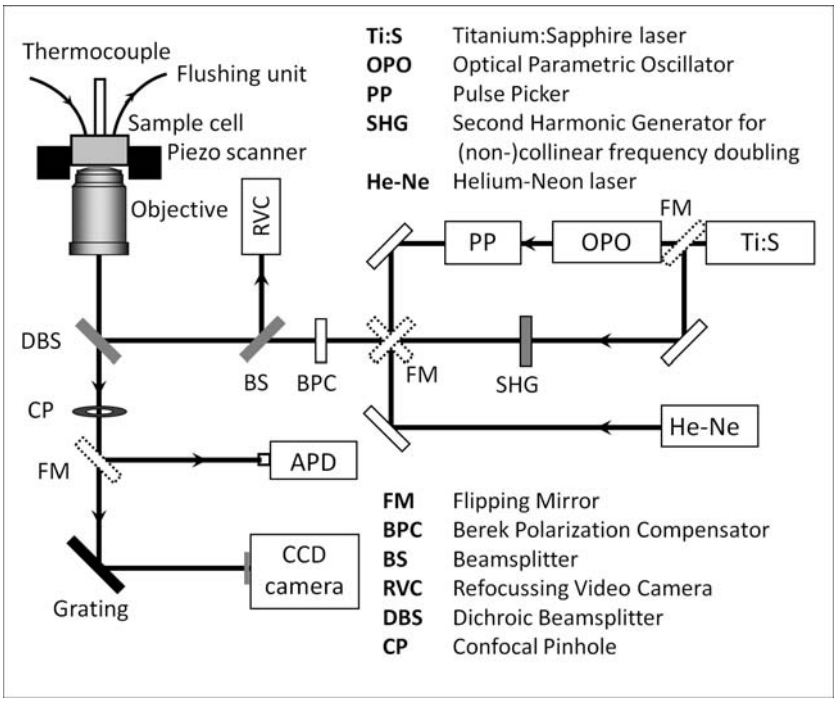

Figure 1.1: Experimental setup

As a light source either a cw laser (He-Ne Melles Griot, 632.8 nm) or a pulsed laser (Ti:Sapphire, Mira 900, 76 MHz, Coherent, 1064 nm) tunable by parametric oscillator (OPO, Coherent) can be used. The light polarization is adjusted to circular by Berek compensator (New Focus) in order to minimize the dependence on the molecules orientation. The beam is spatially filtered by a Kepler telescope with a pinhole to consist of mainly the Gaussian TEM_{00} mode. This achieves more uniform illumination of the molecules and thus reduces the average excitation power needed, hence increasing possible illumination time before photobleaching. The beam, reflected by the dichroic mirror, then enters the inverted microscope (Eclipse TE300, Nikon) and is focused by an objective (Nikon) on the sample cell. The fluorescence is collected by the same objective, passes the dichroic mirror and through the pinhole. Then it can be detected either by avalanche photodiode (APD, SPCM-AQR-16, Perkin-Elmer) for photon counting or dispersed by a grating on the charge-coupled device (CCD, Spec10: 100BR, Princeton Instruments). The sample cell is moved by an automated piezoelectric stage (P713.8-C, Physik Instrumente) and is equipped by a thermocouple for temperature control and stabilization and by a flushing unit, which is needed for flushing the sample with deoxygenated buffer and thus obtaining stable, oxygen-free environment. The laser beam reflected from the sample is used for automated re-focusing by a camera. More detailed account on the setup details together with numerical estimates of the measurement parameters is given in Ref. [10].

1.3 Detected signals

After proper alignment and sample preparation the measurement process is fully automated. The first step is scanning by the piezo stage which results in an image of the scanned area, enabling identification of the single complexes, see Fig. 1.2.

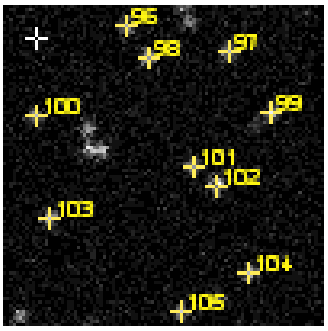

Figure 1.2: Scan image

Based on empirical selection criteria such as size and intensity the single complexes are identified[1]. Then they are measured one by one. As described above, the setup can be used to detect either intensity or spectral traces. In order to obtain sufficient signal-to-noise ratio (SNR), the intensity traces, measured by the APD, are integrated into 10 ms time bins. This results in intensity time traces on the timescale of tens of seconds and time resolution 10 ms, see Fig. 1.3a. For detection of the spectra at the CCD longer integration time of 1 s is needed, see 1.3b.

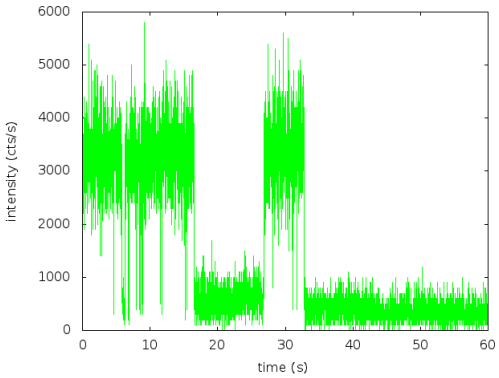

(a) Intensity trace

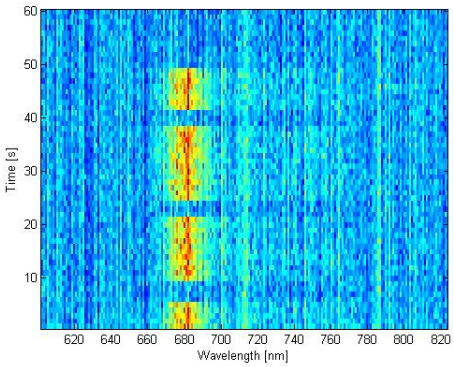

(b) Spectral trace

Figure 1.3: Detected time traces

In the usual setup one spectrum was recorded, followed by a 1 min long intensity trace. From such a measurement the spectral properties distribution is obtained and simultaneously the intensity distributions and blinking statistics are recorded. There is therefore large variety of data available for theoretical simulation and comparison.

[1]Note that if, for example, the blinking was not photoinduced, by this selection we already choose with larger probability the complexes which spend more time in the fluorescent state.

1.4 Sample preparation

The photosystem II complexes were isolated from spinach as described in [12]. The LHCII monomers were then purified using continuous sucrose gradient, centrifugation and gel filtration as also described in [12] and references therein. The purified LHCII monomers were solubilized in a buffer (pH 8, 20 mM HEPES, 1mM $MgCl_2$, 0.03% β-DM) and diluted to required concentration. Then a drop was deposited to a coverglass covered by a layer of poly-L-lysine (PLL, Sigma). The PLL is positively charged and thus binds the complexes to the surfaces, increasing stability[2]. After some time to settle, the sample holder was closed and the sample was flushed by a deoxygenated buffer with added oxygen-scavenging enzymatic system pyranose, pyranose oxidase and catalase. The sample was afterwards cooled to 5 °C to increase the time before photobleaching.

The oxygen scavenging is important since, due to relatively high concentration of chl triplets in the system, a singlet oxygen can be produced [2]. This then aggressively reacts with the system, causing irreversible damage. By removing the oxygen the time before photobleaching is thus extended by an order of magnitude, a requirement necessary for sufficient data collection for subsequent analysis.

1.5 Data analysis

The data were analysed in the following manner:

The individual spectra were fitted by skewed-Gaussian profiles on purely phenomenological basis (see [12] for details), in order to obtain the fluorescence peak positions (FLP) and full-width at half maximum (FWHM). Afterwards the statistics describing the distribution of the FL peaks, their widths and even shifting are available in form of histograms. For our modelling purposes the FLP histograms are of interest.

The intensity traces can be analysed by a correlation function, see section 4.6, for which direct calculation is possible since the noise is uncorrelated. However, because of the relatively limited experimentally accessible timescale (10 ms to 60 s), we believe that in our case the level analysis is more informative. For that purpose a simple algorithm was developed and programmed by Krüger [9]. It utilises the fact that the noise in the signal is Poissonian, which means that the standard deviation should be $\sigma = \sqrt{I}$, where I is the level intensity. Since the signal is binned into 10 ms bins, the distribution of these intensity points should be normal (Gaussian). It is then straightforward to calculate the probability that the deviation of several following points will exceed some multiple of σ. This is tested and, when it does, these next points are treated as a new level. This

[2]The PLL is not necessary. As was experimentally verified, the complexes bind also to clean glass. Because the glass should be negatively charged, the binding could be different (e. g. at different places) and achieving stable complexes after flushing with the buffer is somewhat more complicated. Since we wanted to compare our experiment with the previous results, we used PLL. However, for measurements with chemicals interacting with PLL this could be a possibility.

procedure results in resolved intensity levels with their durations for every trace, see Fig. 1.4 for example (the last level is not analysed since it ended artificially either by photobleaching or end of acquisition time).

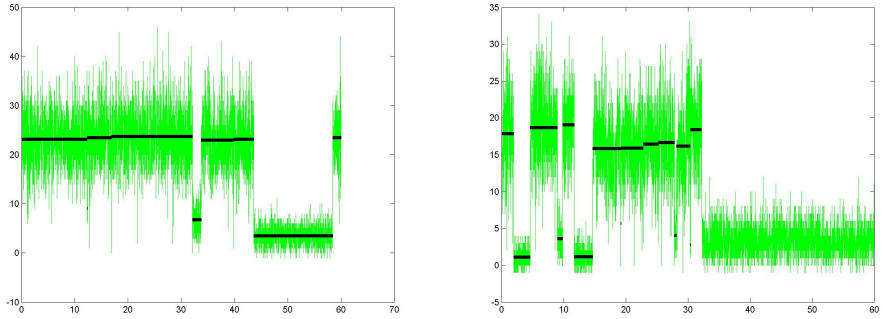

Figure 1.4: Level analysis of the intensity traces

The resolved levels are further analysed, resulting in the switching statistics such as total number of levels, total dwell time in these levels, dwell time distribution for these levels and frequency of accessing them. At this point it is worth noting that the tolerated deviation from the mean intensity of the level must be adjusted by visual control of the trace analysis. This uncertainty in the analysis then can lead to slightly different obtained distributions, especially for the access frequency distribution which will be also used further in the text.

2. Excitonic model

2.1 Introduction

By far the most popular method of describing the spectroscopic properties of molecular aggregates is the excitonic model. Because of the complexity of the biological systems, it would not be feasible to fully quantum mechanically describe the dynamics of the system and its environment to which it is coupled. Instead, we treat the pigments interacting with light (chromophores) which are of interest as an open quantum system. The total Hamiltonian is then traditionally separated as

$$H = H_S + H_{SL} + H_{SB} + H_B, \tag{2.1}$$

where H_S is the system part containing the chromophores and H_{SL} describes their interaction with light. H_B is the bath Hamiltonian including everything else in the environment (e. g. protein, solvent) and H_{SB} is the interaction of the system with the bath.

In the Frenkel exciton model the pigments (in our case chlorophylls) are described by the energies of their electronic transitions and transition dipole moments. The Hamiltonian of each pigment can then be, similarly to (2.1), split into the pigment, pigment-bath and bath part:

$$H_n = H_0^n + H_B^n + H_{SB}^n. \tag{2.2}$$

The pigment part is

$$H_0^n = |\tilde{e}_n\rangle \left(\tilde{\varepsilon}_n + \langle V_e^n - V_g^n\rangle\right) \langle \tilde{e}_n| \otimes \mathbb{I}_B, \tag{2.3}$$

where $\tilde{\varepsilon}_n$ is the excited state energy (for chlorophyll S1 state) and $V_{e/g}^n$ are the potential energy operators of the bath when the system is in the excited/ground state (we set the ground state electronic energy equal to zero for simplicity). The $\langle \bullet \rangle$ means averaging over the bath degrees of freedom (DOF). We can see that the interaction with the bath shifts the excited state energy by $\lambda_n = \langle V_e^n - V_g^n\rangle$. This energy difference is called reorganization energy. The bath part is

$$H_B^n = \left(T_n + V_g^n\right) \otimes \mathbb{I}_S, \tag{2.4}$$

where T_n is the kinetic energy operator of the bath. And the pigment-bath interaction is

$$H_{SB}^n = \left(V_e^n - V_g^n - \langle V_e^n - V_g^n\rangle\right) \otimes |\tilde{e}_n\rangle\langle\tilde{e}_n| = \Delta V_n \otimes |\tilde{e}_n\rangle\langle\tilde{e}_n|, \tag{2.5}$$

where ΔV_n defined by the equation is so-called energy gap function. This typically fluctuates in time and can thus be imagined as the fluctuation of the excited state energy with respect to ground state, which then leads to dephasing of the coherences and gives rise to the lineshape of the transition.

The collective basis states for the molecular system are in this description the ground state $|\bar{g}\rangle = \Pi_n |g_n\rangle$, one-exciton states $|\bar{e}_n\rangle = \Pi_{i\neq n}|g_i\rangle|\tilde{e}_n\rangle$ and multi-exciton states, which are not needed in the linear experiments description. The total Hamiltonian can then be expressed as

$$H = \underbrace{\sum_n H_0^n + \sum_{n<m} J_{nm}|\bar{e}_n\rangle\langle\bar{e}_m|}_{H_S} + \underbrace{\sum_n H_{SB}^n}_{H_{SB}} + \underbrace{\sum_n H_B^n}_{H_B} + \underbrace{\sum_n -\mu_n \cdot E(t)}_{H_{SL}}, \tag{2.6}$$

where we added the Coulombic interaction J_{nm} between the excited pigments and their interaction with light in dipole approximation, which is completely justified in the systems of interest where the incident light wave is at least order of magnitude longer than the size of the system. The transition dipole operator μ_n couples the ground state and one-exciton manifold: $\mu_n = |\bar{g}\rangle\mu_{0n}\langle\bar{e}_n| + h.c.$ (h.c. denotes Hermitian conjugate). When we consider the one-exciton block of the Hamiltonian from (2.6) we can see that in this basis of individual excited pigments, so called site basis, the off-diagonal terms are only the inter-pigment couplings. The site basis is therefore the preferred basis when the coupling between the pigments is weak compared to their interaction with the bath. The excitation then tends to be localized on the individual pigments. In the system dynamics a perturbation theory in J can than be used, leading to Förster energy transfer [21].

However, in most photosynthetic antenna systems the coupling between the pigments is stronger or at least comparable to the interaction with bath. The preferred basis is then the so called exciton basis, in which the system Hamiltonian H_S is diagonal. The states obtained after the diagonalizing orthogonal transformation are called excitons, and they are linear combinations of the site basis vectors: $|e_i\rangle = \sum_n c_i^n |\bar{e}_n\rangle$ [32]. Here c_i^n are coefficients of the orthogonal transformation matrix:

$$\sum_{nm} c_i^{*n} \left(H_S\right)_{nm} c_j^m = \delta_{ij}\varepsilon_i, \tag{2.7}$$

ε_i being the excitonic energies. The excitation is in this case delocalized over several pigments. When describing the system dynamics, the perturbation theory in H_{SB} can be used. The excitation energy transfer (EET) can described by (Modified) Redfield theory [21].

In the intermediate regime the two approaches described above can also be combined. The strongly coupled pigments then form excitonic blocks in the Hamiltonian and are diagonalized separately. The energy transfer inside these blocks can then be described by (Modified) Redfield theory, while the transfer between the blocks can be described by generalized Förster rates [18]. Nevertheless, it should be mentioned here that even this approach is not exact since it, for instance,

does not include polaron localization effects and also the distinction between the blocks is made by introducing some phenomenological coupling cutoff.

2.2 Towards SMS

In the SMS experiments the time-resolved fluorescence of the molecules can be observed. In the excitonic model the fluorescence (FL) is given by the steady state excitonic populations values. In this section we therefore present a derivation of equations for populations evolution. There was an extensive work done in the last years in accurately describing the system dynamics when illuminated by light and in contact with bath, for a good starting point for overview and further reading see [30] . The commonly used equations, which are derived from Liouville - von Neuman equation for the density matrix (DM), describe the complete system DM evolution starting from the femtosecond time scale and are therefore suitable for description of ultrafast experiments. However, on the timescale relevant in SMS which goes to tens of seconds, the implementation of these equations is not computationally feasible and even appropriate, for we argue, see further discussion, that the transient effects have a little importance in the long time, steady state population dynamics, which plays role under mentioned experimental conditions. We here therefore derive approximative equations for the populations dynamics only, applicable on the timescale from tens of picoseconds to tens of seconds.

We start with convolution-less master equation for the reduced density matrix (RDM):

$$\frac{\partial}{\partial t}\rho(t) = -\frac{i}{\hbar}[H_S + H_{SL}, \rho(t)] - \mathcal{R}(t)\rho(t). \tag{2.8}$$

Here $\rho(t) = Tr_B W(t)$ is the reduced DM (RDM), which is obtained by tracing the full DM over the bath DOF. $\mathcal{R}(t)$ is then some (fourth rank) relaxation tensor acting on the RDM. Presence of this term is a consequence of the reduced description and its components connect different terms of the RDM, expressing population transfer etc. The form of the tensor depends on the basis used and approximations employed.

In our theory we use the secular approximation (no direct transfer between populations ρ_{ii} and coherences ρ_{ij}) and linear regime in interaction with the electrical field. Then we can write explicitly the elements (either in site or exciton basis) of the RDM, getting the following coupled equations (we set $\hbar = 1$ in the following text for simplicity):

$$\frac{\partial \rho_{ii}}{\partial t} = \sum_j k_{ij}\rho_{jj} - \Gamma_i \rho_{ii} + (i\mu_{i0}\rho_{0i}(t)E(t) + c.c.) \tag{2.9}$$

$$\frac{\partial \rho_{i0}}{\partial t} = -i\omega_{i0}\rho_{i0} - \mathcal{R}_{i0i0}(t)\rho_{i0}(t) + i\mu_{i0}(\rho_{00} - \rho_{ii})E(t) \tag{2.10}$$

Here ω_{i0} is the energy of the i-th state with respect to ground state, k_{ij} are transfer rates between populations (from j to i), $\Gamma_i = \tilde{\Gamma}_i + \sum_j k_{ji}$ is population decrease

rate given by population relaxation to the ground state $\tilde{\Gamma}_i$ and transfer to another state. We assume that the population transfer rates are time-independent, an approximation frequently used even on the ultrafast timescale.

The equation of motion for the coherences (2.10) can be solved by the method of Green functions. First we solve with a delta function instead of the laser field:

$$\frac{\partial G_i(t)}{\partial t} + i\omega_{i0}G_i(t) + \mathcal{R}_{i0i0}(t)G_i(t) = \delta(t) \tag{2.11}$$

A solution is a free (meant without the interaction with the electrical field) propagation starting at $t = 0$:

$$G_i(t) = \theta(t)\mathcal{U}_{i0i0}(t). \tag{2.12}$$

The field-induced coherence is then given by a convolution of the field with this Green function

$$\rho_{i0}(t) = i\mu_{i0}\int_0^{t-t_0} d\tau G_i(\tau)[\rho_{00}(t-\tau) - \rho_{ii}(t-\tau)]E(t-\tau). \tag{2.13}$$

At this point we need to make some more approximations. The main idea is that because in the biological systems the pure dephasing is much faster than the population relaxation, we can assume that the populations remain constant during the integration. Moreover, we can send the upper limit of the integration to infinity. This assumption is valid under two conditions: the pure dephasing must really be much faster than the population dynamics and the changes in the environment and the laser field must be slow. In other words, if the typical dephasing time is τ_D, this approximation holds for $t \gg \tau_D$. It can be looked at as a coarse graining of the time axis into the intervals given by optical coherences lifetime. The typical timescale for the optical coherences dephasing in systems of interest is in the order of ∼100 fs [15] so this description is completely suitable for the SMS, where the time resolution typically starts from ms.

Considering the requirements listed above fulfilled, we can write

$$\rho_{i0}(t) = i\mu_{i0}[(\rho_{00}(t) - \rho_{ii}(t)]\int_0^{\infty} d\tau E(t-\tau)\mathcal{U}_{i0i0}(\tau), \tag{2.14}$$

Note that when we are concerned about the steady state, $\dot{P}_i = 0$, then taking the populations out of integration can be regarded as exact. Shifting the upper bounds of integration is then for any relevant times completely justifiable.

We are ready now to insert this expression for optical coherences into the equation for populations (2.9), obtaining

$$\frac{\partial P_i(t)}{\partial t} = \sum_j k_{ij}P_j(t) - \Gamma_i P_i(t) + |\mu_{i0}|^2(P_0(t) - P_i(t))\int_0^{\infty} d\tau E(t)E(t-\tau)\mathcal{U}_{i0i0}(\tau). \tag{2.15}$$

Now let us trace over the field degrees of freedom if we treat it quantum-mechanically or just take an expectation value in the semi-classical treatment, for more detailed treatment see [14]. Then we can employ the fact that $\langle E(t)E(t-\tau)\rangle$ is a light correlation function and its Fourier transform is a power spectrum of the light [8, 3],

$$\langle E(t)E(t-\tau)\rangle = \int_0^\infty d\omega W(\omega) e^{i\omega\tau}. \tag{2.16}$$

Switching the order of integrations and using the definition of absorption lineshape of the i-th pigment/exciton [17],

$$\chi_i(\omega) = |\mu_{i0}|^2 \int_0^\infty d\tau e^{i\omega t} \mathcal{U}_{i0i0}(\tau), \tag{2.17}$$

we finally arrive at

$$\frac{\partial P_i}{\partial t} = \sum_j k_{ij} P_j - \Gamma_i P_i + (P_0 - P_i) \int d\omega W(\omega)\chi_i(\omega), \tag{2.18}$$

To summarize this part, what we get is a closed set of equations for populations only. The population changes are given by the transfer rates between populations, population relaxation and the source terms expressed as an overlap of the excitonic/pigment spectra with the light spectrum.

Moreover, the equations have constant coefficients and therefore can be written in the form

$$\frac{\partial \mathbf{P}}{\partial t} = \mathcal{M}\mathbf{P} + \mathbf{S}, \tag{2.19}$$

where $\mathcal{M}$ is a matrix of relaxation, population transfer rates and $\mathbf{S}$ are the source terms. This equation can be solved analytically:

$$\mathbf{P}(t) = \mathcal{M}^{-1}(e^{\mathcal{M}t} - 1)\mathbf{S} + e^{\mathcal{M}t}\mathbf{P}(t=0). \tag{2.20}$$

This enables us to express the populations values in any time starting from ps without solving for all the previous times, making it possible to explain experiments where more different timescales are important, such as single-molecule spectroscopy. Indeed, when describing the non-photochemical quenching, the relevant switching mechanisms operate on scale of miliseconds to seconds and the change of parameters such as protein conformation can cause population transfer in order of tens to hundreds of picoseconds to quench the fluorescence, the fluorescent lifetime of chlorophylls being in order of nanoseconds.

We should also note here that the saturation of absorption term $(P_0 - P_i)$ in eq. (2.18) should be, when strictly staying in the linear regime, set equal to one. This also means that the approximative treatment of (2.13) is justified. If we wanted to include the non-linear effects we should also consider more than one

excitation present and in the optical coherences evolution there would appear $\frac{\partial \rho_{io}}{\partial t} \sim \mu_{j0}\rho_{ij}E$ terms, which result in mixing of the electronic coherences with the populations even when staying in the secular approximation. In our calculations we thus always consider sufficiently weak light (condition which must be checked when comparing to experimental data) in order to stay in the linear regime.

Once we know the steady state populations P_i, we are ready to calculate the fluorescence and hence also the SMS signal, see section 4.3.

3. Protein conformation switching model

As mentioned in the introduction, the blinking statistics alone can be well described by a two-level model proposed by Valkunas *et al.* [31]. In this chapter we present the equations to describe the protein switching between two conformational states. The basic idea is that by random fluctuations the protein samples its potential energy surface (PES) doing a random walk (RW). It is supposed there are two stable conformations of the protein and, correspondingly, the PES have two minima, which are approximated by two harmonic potentials by quantum tunnelling. The protein then does a RW in this potential, and at every point it has some probability to switch to the second potential. The ratio between the upward/downward rate reflects the detailed balance condition, i. e. the probability of residing on the two surfaces at given coordinates point is given by the Boltzmann equilibrium according to the surface energies.

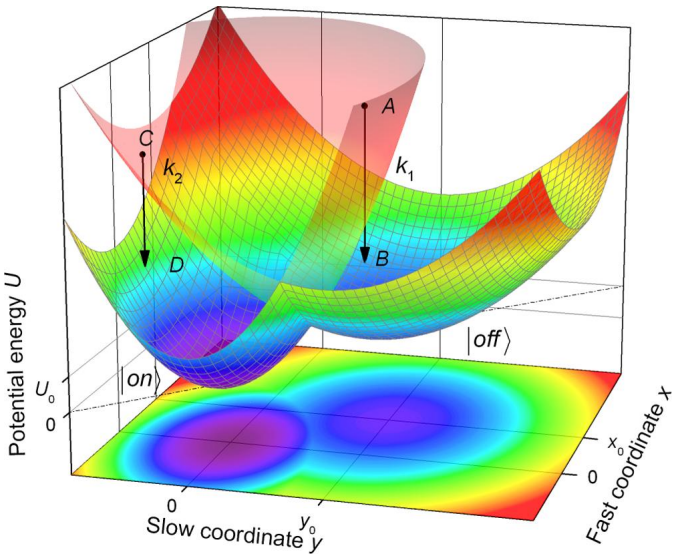

Figure 3.1: Protein PES, taken from [31]

The two PES minima corresponding to the |on> (1) and |off> (2) states can be in the first approximation modelled as two harmonic potential wells projected on two generalized coordinates, see Fig. 3.1:

$$\begin{aligned} U_1 &= \frac{1}{2}\lambda_1 x^2 + \frac{1}{2}\gamma_1 y^2 \\ U_2 &= \frac{1}{2}\lambda_2 (x - x_0)^2 + \frac{1}{2}\gamma_2 (y - y_0)^2 + U_0. \end{aligned} \tag{3.1}$$

Here the y coordinate is the relatively slowly varying conformational coordinate and x includes all other fast protein fluctuations. The λs and γs are reorganization energies in the potentials along respective coordinates and the minima are located in $(0, 0)$ and (x_0, y_0) with an energy distance U_0 between them.

3.1 Continuous probability description

Following the original description by Valkunas in Ref. [31] and, in more detail, in Ref. [4], we can describe the protein using the probability density. The equation of diffusive motion on the potential surfaces for the probability density ρ of being at point (x, y) on the $i-th$ potential in time t is a Smoluchovski equation with additional term representing the possibility of tunneling to the other potential surface:

$$\frac{\partial \rho_i(x,y,t)}{\partial t} = \left[D_{ix}\mathcal{L}_x + D_{iy}\mathcal{L}_y - k_i H_i(x,y)\right]\rho_i(x,y,t), \tag{3.2}$$

where Ds are the diffusion coefficients on respective potentials in respective coordinates, $\mathcal{L}s$ are diffusion operators

$$\mathcal{L}_z\rho_i(x,y,t) = \left[\frac{\partial^2}{\partial z^2} + \frac{1}{k_B T}\frac{\partial}{\partial z}\frac{\partial U_i}{\partial z}\right]\rho_i(x,y,t),\ i=1,2;\ z=x,y, \tag{3.3}$$

k_i is the falling rate from the $i-th$ potential and

$$\begin{aligned} H_1(x,y) &= e^{-\alpha|\Delta U|/\hbar\omega_0}\min\{1, e^{(U_1-U_2)/k_BT}\}, \\ H_2(x,y) &= e^{-\alpha|\Delta U|/\hbar\omega_0}\min\{1, e^{(U_2-U_1)/k_BT}\} \end{aligned} \tag{3.4}$$

represent the tunneling probabilities reflecting energy gap law (1st term) and detailed balance condition (the min term). α can be treated as a constant and ω_0 is a characteristic frequency of the protein environment vibrations responsible for the tunneling. Because the diffusion along the x coordinate is by definition much faster it can be adiabatically eliminated from the equation:

$$\frac{\partial \rho_i(y,t)}{\partial t} = \left[D_{iy}\mathcal{L}_y - \kappa_i(y)\right]\rho_i(y,t), \tag{3.5}$$

where

$$\begin{aligned} \kappa_1(y) &= k_1\sqrt{\tfrac{\lambda_1}{2\pi k_BT}}\int dx e^{-\frac{1}{2k_BT}\lambda_1 x^2} H_1(x,y) \\ \kappa_2(y) &= k_2\sqrt{\tfrac{\lambda_2}{2\pi k_BT}}\int dx e^{-\frac{1}{2k_BT}\lambda_2 (x-x_0)^2} H_2(x,y) \end{aligned} \tag{3.6}$$

come from the long-time equilibrium condition in x diffusion. Because we want to use as simple description as possible, we set the potentials in the direction of the fast coordinate x the same in the on and off state, i. e. $x_0 = 0$, $\lambda_2/\lambda_1 = 1$. As $H_{1,2}$ depend only on the distance of the potentials, there is no x-dependent term in them and the remaining Gaussian term in (3.6) is easily integrated over. There are two reasons for this treatment. First, the tunneling rates do not have to be integrated over x simplifying the calculation, and second, more importantly, we

believe that, in the spirit of Occam's razor, the simplest model which correctly describes all the desired features should be used.

After transforming into dimensionless coordinates $y\sqrt{\frac{\gamma_1}{k_BT}} \to y$ and eliminating x, the potentials for the on (1) and off (2) state are

$$\begin{aligned} \frac{U_1}{k_BT} &= \frac{1}{2}y^2, \\ \frac{U_2}{k_BT} &= \frac{1}{2}\frac{\gamma_2}{\gamma_1}\left(y-y_0\right)^2 + \frac{U_0}{k_BT}. \end{aligned} \tag{3.7}$$

The jumping probability rates are now simply

$$\begin{aligned} \kappa_1(y) &= k_1 \quad e^{-\alpha|\Delta U|/\hbar\omega_0}\min\{1, e^{(U_1-U_2)/k_BT}\}, \\ \kappa_2(y) &= k_2 \quad e^{-\alpha|\Delta U|/\hbar\omega_0}\min\{1, e^{(U_2-U_1)/k_BT}\}. \end{aligned} \tag{3.8}$$

The situation is now equivalent to the case where we started only with the slow coordinate y.

The initial condition can chosen in the following way: $\rho_2(y,0) = \rho_1^{st}(y)\kappa_1(y)$, where $\rho_1^{st}(y)$ is the steady state solution on U_1 potential without tunneling. The $\rho_1(y,0)$ is chosen analogically and, as the authors point out in [31], it is interesting that after normalizing the initial distributions coincide and the distribution is a sharp peak. This condition corresponds to the system in equilibrium at the beginning of every calculated dwell time.

The survival probability is the overall probability that the protein stays on the respective surface:

$$S_i(t) = \int dy \rho_i(y,t). \tag{3.9}$$

The probability of the transition corresponding to the experimentally obtained blinking statistics is then

$$P_i(t) = -\frac{dS_i(t)}{dt}. \tag{3.10}$$

This continuous probability distribution description was used by Valkunas and originally also for the purpose of this work. However, we believe that it is better to solve this problem as a discrete RW for two reasons. First, the equations (3.2) can be solved uncoupled this way only for conditioned probabilities, i.e. assuming that the system was in the opposite state in the previous interval, and, in the same time, employing the same, equilibrium initial condition for each dwell time. When continuously modelling the trajectory of a single protein, we do not have to include the resetting after switching and also the conditioning will be inherent, as the system is observed being in the particular state. And second, when we want to simulate the individual intensity time traces, it is more natural to really follow the trajectories of the individual proteins on their PES.

3.2 Discrete RW description

As mentioned above, if we want to follow the time trace of every single molecule, we should follow its particular trajectory. The blinking statistics will then be recovered by averaging over a large number of molecules, exactly as in the experiment. To the purpose of following the trajectory of the individual proteins, we need to describe its discrete RW (DRW) in the potential. We will denote probability of going right (left) as p (q). In the symmetrical RW we have $p = q = \frac{1}{2}$. If the protein is at coordinate y, in the next step it will move with probability p to $y + a$ and with probability q to $y - a$, where a is the length of the step. Inspired by classical approach by van Kampen [33], we augment the position dependent probabilities in the presence of the potential $U(y)$ as

$$p(y) = \frac{1}{2} e^{-\frac{1}{k_B T}(U(y+a)-U(y))}, \tag{3.11}$$

$$q(y) = \frac{1}{2} e^{-\frac{1}{k_B T}(U(y-a)-U(y))}. \tag{3.12}$$

We note that thus defined probabilities reflect the detailed balance condition $\frac{p(y)}{q(y)} = e^{-\frac{1}{k_B T}(U(y+a)-U(y-a))}$. Considering small step a, we can use Taylor expansion in y $\left(e^{-\frac{1}{k_B T}U(y\pm a)} \approx e^{-\frac{1}{k_B T}U(y)}\left(1 \mp \frac{1}{k_B T}\frac{dU}{dy}(y)a\right)\right)$, obtaining for the difference of the probabilities

$$p(y) - q(y) = -\frac{1}{k_B T}\frac{dU}{dy}(y)a. \tag{3.13}$$

Now considering that $p(y) + q(y) = 1$, we get

$$p(y) = \frac{1}{2} - \frac{1}{2k_B T}\frac{dU(y)}{dy}a. \tag{3.14}$$

Using the potential form (3.7), we get for the probabilities

$$\begin{aligned} p_1(y) &= \frac{1}{2} - \frac{1}{2k_B T} y a_1, \\ p_2(y) &= \frac{1}{2} - \frac{1}{2k_B T}\frac{\gamma_2}{\gamma_1}(y - y_0)a_2. \end{aligned} \tag{3.15}$$

The length of the step a on respective surface can be related to the transformed diffusion coefficient $D_{1,2}$:

$$a_{1,2} = \frac{D_{1,2}\gamma_1}{k_B T}\Delta t, \tag{3.16}$$

where Δt is the time duration of the step.

When we want to obtain the blinking statistics, we follow exactly the same procedure as in the experiment - we simulate many single trajectories and then analyze them.

4. LHCII as a typical photosynthetic antenna system

4.1 Role in photosynthesis

Photosynthesis is a process by which plants, algae and some bacteria fix carbon from atmosphere into organic compounds using energy from sunlight. To capture the energy, photosynthetic organisms have developed sophisticated pigment-protein antenna complexes which absorb light and transport the excitation energy to the reaction center (RC) where the charge separation, the first step of a complex series of reactions, takes place. This produced charge is transported along the membrane and creates a pH gradient, which is a driving force in subsequent reactions [2]. Light harvesting complex II (LHCII) is a peripheral antenna system of higher plants and algae, associated with photosystem II (PS2)[1]. Under physiological conditions PS2 binds 6 LHCII trimers. LHCII is the most abundant membrane protein on Earth and contains more than half of the chlorophylls in the leaves of higher plants and algae [5, 10]. As its primary function is light harvesting, it has high absorption cross section (approx. 17 $Å^2$ for the trimers [10]), which makes it also ideal as a subject of SMS study.

The main function of the LHCs including LHCII is the light absorption and subsequent energy transfer. However, the light conditions vary during the day and it is not always advantageous and possible for the plant to utilise all harvested sunlight. On the contrary, accumulation of excited pigments under excess illumination due to slow turnover rate of the RC can lead to formation of dangerous radicals, which in turn can damage the LHCs. To prevent these unfortunate consequences, the plants have developed several photoprotective mechanisms which reduce light absorption and deal with excess energy. Collectively these mechanisms are called non-photochemical quenching (NPQ), named after the effect on observed fluorescence. NPQ mechanisms can be divided by roughly their speed into fastest energy-dependent quenching (qE) governing energy dissipation, slower state transition (qT), see footnote 1, and slowest intensity dependent part (qI), including repair mechanisms. In the context of our work the qE part is of interest. It has been much speculated in the last years about the nature of NPQ in PS2 and its connection to carotenoids and the xanthophyll cycle, for good review focused on LHCII see [27]. Currently it seems that at least part of the scientific community agrees that energy transfer to carotenoid lutein, which is also part of LHCII, could be involved. This would mean that the transition between the light-harvesting and photoprotective mode happens already on the level of the antenna systems. This suggestion is, thanks to SMS, also supported by experimental observations and now by the results of this thesis.

[1] This fully applies in state I. After state transition into state II two LHCII can detach and associate with photosystem I. This serves as a light-harvesting regulation mechanism, compensating the energy income of the two photosystems.

From 2004 the crystal structure of LHCII is known at 2.72 Å resolution [13], which provides sufficient information about the pigment composition and orientation, an excellent starting point for theoretical modelling. LHCII naturally occurs in trimeric form and each monomer contains 8 chlorophylls a, 6 chlorophylls b, two luteins, one neoxanthin and one carotenoid of the xanthophyll cycle (zeaxanthin or violaxanthin). For the structure and pigment numbering, which is also used throughout this text, see Fig. 4.1. For experimental use either trimeric or monomeric form can be purified, see section 1.4.

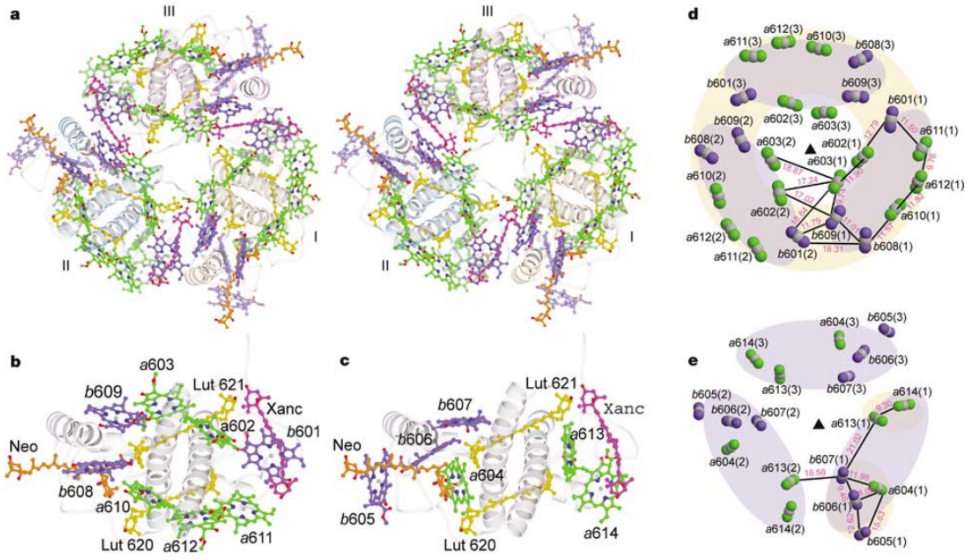

Figure 4.1: Structure of LHCII, taken from Ref. [13]
***a**, LHCII trimers, view from the stromal side, normal to the membrane, monomers labeled I-III. green: chl a, blue: chl b, yellow: lutein, orange: neoxanthin, magenta: xanthophyll-cycle carotenoids. **b** resp. **c**, pigments in monomeric unit at stromal resp. lumenal side. **d** and **e**, arrangement of chls at stromal and lumenal side. gray atom: central Mg, two green (blue) atoms: chl a (chl b) nitrogens in Qy transition direction. numbers: center-center distances in Å*

Because of its biological importance LHCII has been thoroughly studied by many experimental methods in the past decades. From the optical spectroscopy methods we can mention absorption, fluorescence, transient absorption, linear and circular dichroism, see Ref. [18] and references therein, Stark spectroscopy [34] and also 2D spectroscopy [28]. Finally, also SMS measurements on LHCII under various conditions were made, which were also the motivation for this this thesis.

4.2 SMS experiments

The first single-molecule fluorescence measurements on isolated LHCII trimers and monomers was reported by group in Stuttgart in 2001 [29]. Their results for the monomers showed fluorescence peak around 681.3 nm with relatively high degree of polarization. From this they conclude that the emission peak is dominated

by one emitter. As we will see further, this is consistent with our modelling.

Starting from 2010, SMS experiments on LHCII were performed by Krüger at VU Amsterdam [10]. They revealed several interesting features including spectral diffusion/switching together with appearance of very red emission states, and fluorescence intermittency on timescale ranging from 10 ms to 10 s. Furthermore, the dependence of this features on the environmental conditions was studied. It was shown by Krüger, Novoderezhkin *et al.* that the spectral peak shapes and distribution can be explained by an excitonic model[12]. The red states above 700 nm and wide double-peaks with a red component can not be explained by this model, and it is speculated that mixing with the charge transfer (CT) states can be involved. To explain the blinking behaviour a switching model was developed by Valkunas and coworkers[31, 4], see section 3. The idea is that, by a protein conformational change, the complex switches between radiative and dissipative state. Since the dark states were stabilised under conditions corresponding to high-illumination conditions in vivo, it is speculated that the switching is connected to the photoprotective NPQ.

4.3 Excitonic structure

To model spectroscopic properties of the LHCII, including absorption and fluorescence, we have to construct the system parts of the Hamiltonian (2.6). For practical reasons in our spectral window it is enough to consider only the Q_y transitions of the chlorophylls. Because of the different protein environment, the $S_0 - S_1$ transition energy of each chlorophyll is different, i.e. each pigment has different site energy $\tilde{\varepsilon}_n$. As the linear spectra at room temperature are not very sensitive to exact values of the site energies, we do not attempt their fitting and instead we take the values from [21]. The effective transition dipole strength was chosen 3.4 D for Chl b and 4.0 D for Chl a, the dipole orientations and distances are taken from the PDB file based on the crystal structure [13]. The coupling J between the pigments is calculated in the dipole-dipole approximation. The system Hamiltonian can be found in Table A.1 in Appendix A.

We treat the interaction with the environment by second order perturbation theory. The bath is then completely described by its correlation function. The real part of the correlation function in the spectral domain represents the spectral density of the bath vibrations. We use the spectral density from [19], originally obtained by fitting of the fluorescence line narrowing spectrum. It is constructed from one overdamped oscillator representing the slow protein vibrations and several high-frequency pigment modes:

$$C''(\omega) = 2\lambda_0 \frac{\gamma_0 \omega}{\omega^2 + \gamma_0^2} + \sum_{i=1}^{48} 2S_j \omega_j \frac{\omega_j^2 \gamma_j \omega}{(\omega^2 - \omega_j^2)^2 + \omega^2 \gamma_j^2}. \tag{4.1}$$

The spectral dependence of $C''(\omega)$ is depicted in Fig. A.1 in Appendix A. The (temperature dependent) correlation function given by this spectral density is

assumed to be uncorrelated between individual sites and differs only between Chl a and Chl b, while the difference is only in the coupling strength $\nu_n = \nu_{a/b}$:

$$C_n(\omega) = \nu_n C(\omega) = \nu_n \left(1 + \coth\left(\frac{\hbar\omega}{2k_B T}\right)\right) C''(\omega). \tag{4.2}$$

The time-dependent correlation function is then obtained by Fourier transform of (4.2). The difference between the vertical, Franck-Condon transition of the pigments, which are called site energies in this text, and their 0-0 transitions is given by the reorganization energy due to the interaction with the bath:

$$\lambda = \frac{1}{\pi} \int_0^\infty \frac{C''(\omega)}{\omega}. \tag{4.3}$$

Because the pigments are strongly coupled, the preferred basis is the excitonic basis. The system Hamiltonian is diagonal in this basis, the eigenvalues being the exciton energies ω_{i0}. Everything is transformed into this basis by the transformation matrix with coefficients c_i^n, see Eq. (2.7) in section 2.1:

$$C_i(t) = \sum_n |c_i^n|^2 C_n(t), \tag{4.4}$$

$$\mu_{i0} = \sum_n c_i^n \mu_{n0}. \tag{4.5}$$

Note here the linear summation of the transition dipole moments. This leads to the redistribution of the oscillator strength $|\mu_{i0}|^2$ of the transitions, giving rise to dim and superradiant states.

The reorganization energy λ_i due to the interaction with the phonons in the bath is smaller in the exciton basis:

$$\lambda_i = \sum_n |c_i^n|^4 \nu_n \lambda. \tag{4.6}$$

The zero phonon lines are then

$$\omega_{i0}^{ZPL} = \omega_{i0} - \lambda_i, \tag{4.7}$$

where ω_{i0} is the transition frequency of $i-th$ exciton.

The lineshapes are calculated by 2nd order cumulant expansion employing so-called lineshape functions:

$$g_{ii}(t) = \int_0^t d\tau \int_0^\tau d\tau' C_i(\tau'). \tag{4.8}$$

Conveniently the lineshape can be expressed by the spectral density

$$g_{ii}(t) = \frac{1}{\pi}\int_0^\infty d\omega \frac{C_i''(\omega)}{\omega^2}\left[\coth\left(\frac{\hbar\omega}{2k_BT}\right)(1-\cos(\omega t)) + i\,(\sin(\omega t) - \omega t)\right]. \quad (4.9)$$

The absorption spectrum is then calculated as

$$abs(\omega) \propto \omega \sum_i \chi_i(\omega), \quad (4.10)$$

where the absorption lineshape, already defined in (2.17), is

$$\chi_i(\omega) = |\mu_{i0}|^2 \int_0^\infty d\tau\, e^{-i(\omega-\omega_{i0})\tau - g_{ii}(\tau) - \frac{\Gamma_i}{2}\tau}. \quad (4.11)$$

The fluorescence is calculated as

$$FL(\omega) \propto \omega \sum_i P_i \tilde{\chi}_i(\omega), \quad (4.12)$$

where the fluorescence lineshape is given by (see Ref. [17])

$$\chi_i(\omega) = |\mu_{i0}|^2 \int_0^\infty d\tau\, e^{-i(\omega-\omega_{i0}+2\lambda_i)\tau - g_{ii}^*(\tau) - \frac{\Gamma_i}{2}\tau}. \quad (4.13)$$

Note here the Stokes shift $2\lambda_i$ from the absorption line.

The population transfer rates are calculated by the Redfield theory,

$$k_{ij} = \sum_n |c_i^n|^2 |c_j^n|^2 C_n(\omega_{i0}^{ZPL} - \omega_{j0}^{ZPL}) \quad (4.14)$$

and, for comparison, also by the so-called Modified Redfield theory, see e.g. Ref. [19]. Since there is almost no difference between the Redfield and Modified Redfield calculation results in evaluating the quantities of interest in our thesis, the Redfield model is used, because of its smaller computational demands.

The population relaxation rates of chlorophylls $\Gamma_i = \sum_j k_{ji} + \tilde{\Gamma}_i$, where $\tilde{\Gamma}_i = \sum_n |c_i^n|^2 \tilde{\Gamma}_n$ and $\tilde{\Gamma}_n$ were taken to be 3 ns $\forall n$. The equations (2.18) allow us to use light of any spectrum, here we use spectrally narrow (laser) constant illumination at 630 nm with arbitrary, weak intensity in order to stay in the linear regime. In Fig. 4.2 we can see the absorption and fluorescence spectra together with the populations dynamics in exciton and also site basis.[2] The calculations were done at 5°C reflecting the experimental conditions and all values were averaged

[2]We note that transforming back into site basis we should include also terms $\rho_{nn} = c_{nj}c_{in}^*\rho_{ij}$, which include excitonic coherences which are not included in our model. Neglecting these values the site populations become only sums of excitonic populations weighted by the participation ratio of given pigment in the excitons and should thus be treated as being useful more for interpretative reasons.

over 85 cm^{-1} wide disorder in the site energies. The lines are calculated values, the points are experimental results taken from Ref. [12]. Although the blue chl b shoulder is not perfectly reproduced, from the FL spectrum we conclude that our excitonic model is good enough for our purpose. When looking at the excitonic composition of the FL spectrum and at the population dynamics, we can see that the most populated are the lowest three excitons, which are formed by strongly coupled pigments chl 610-611-612, chl 602-603 and chl 613-614 (see Fig. 4.1 for numbering). This is in agreement with previous modelling results for LHCII [20]. Also the FL peak is dominated by the lowest exciton which resides on the 'terminal emitter' group of chl 610-611-612. This is in agreement with the polarization measurements from Ref. [29].

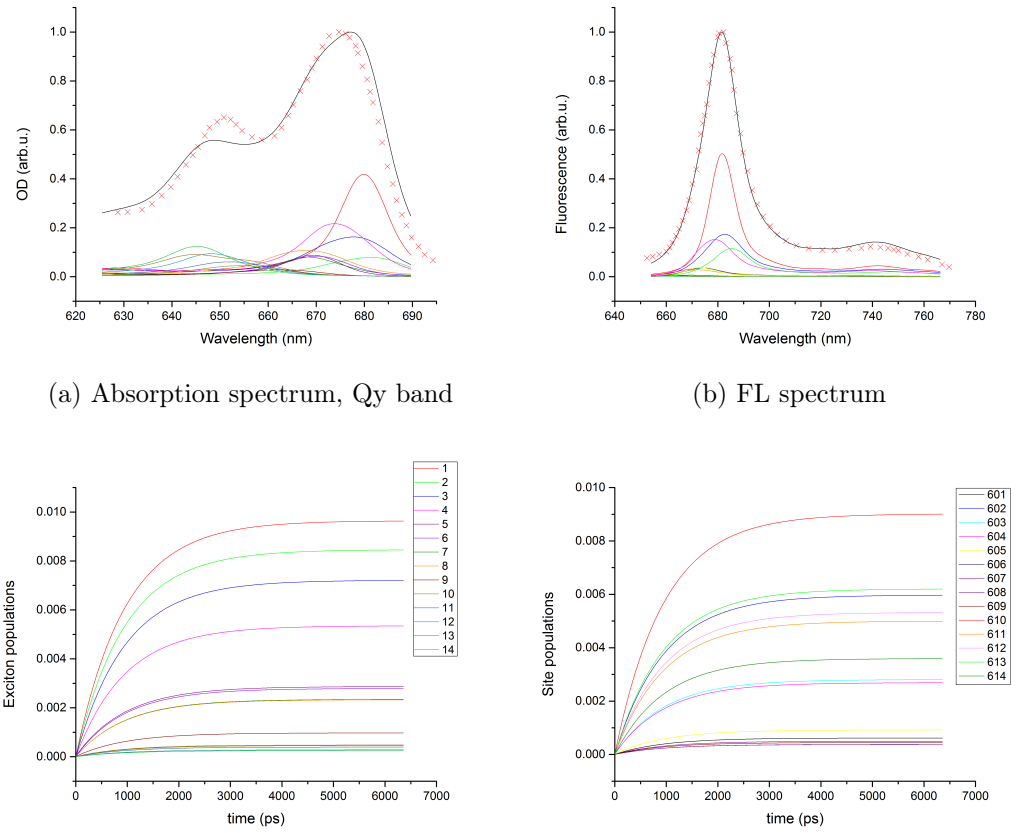

(a) Absorption spectrum, Qy band

(b) FL spectrum

(c) Ecitonic populations dynamics

(d) Site populations dynamics

Figure 4.2: Excitonic model

When we know that our model works in the bulk sample, we can try to reproduce the statistics from the SMS experiments. In Fig. 4.3 there is the FL spectral peak distribution compared to the experiment. We can see that it is little broader but fits quite well. This means that not only the averaged population dynamics but also its individual realizations are in agreement with the experiment.

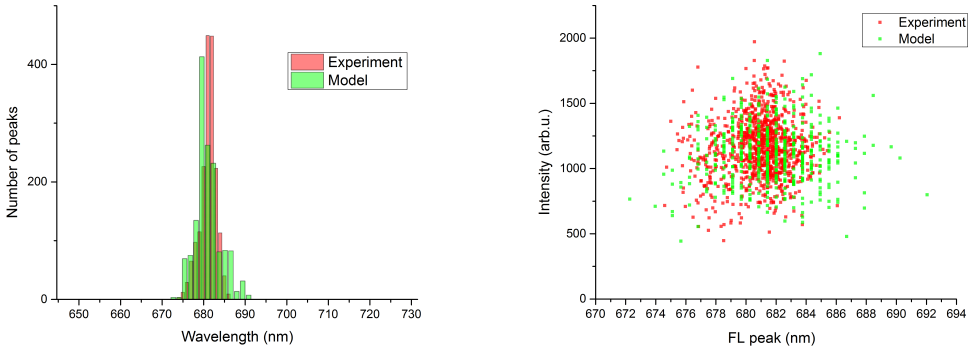

(a) FL peak position

(b) Intensity vs FL peak position

Figure 4.3: FL peak distribution

Now it is time to look at the intensity traces. However, since they exhibit significant amount of blinking, i. e. reversible switching to the off state, we should focus on including some fluorescence quenching mechanism first.

4.4 Energy dissipation and NPQ

Because of the broad on/off state duration timescale, it is probable that the excitation energy is dissipated. In the same time, the energy-dependent, fastest component of NPQ, qE, is argued to work by rapidly dissipating the excitation energy before it reaches the RC. It therefore makes sense to try to implement a proposed NPQ mechanism and see if it can cause fluorescence blinking in the required extent. One mechanism of FL quenching in LHCII, proposed by Ruban and coworkers, is an energy transfer to Lut 1 (lut620), which is in the vicinity of the 'terminal emitter' group of chlorophylls a610-611-612 and is supposed to be coupled mainly to chl a612 [26, 6]. The Lut S1 state is optically forbidden and has short (10 ps) non-radiative decay lifetime [24], so it could in principle act as a quencher. This was also the conclusion of the Ruban's work, see Fig. 4.4b.

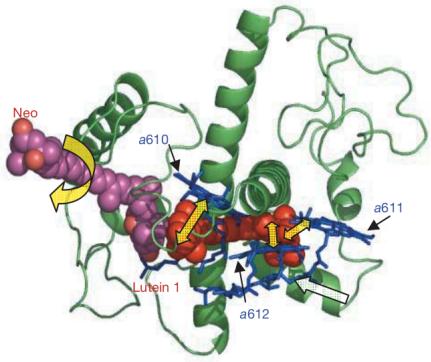

(a) Lutein Lut 1 position near chl a 610-611-612 cluster, taken from [26]

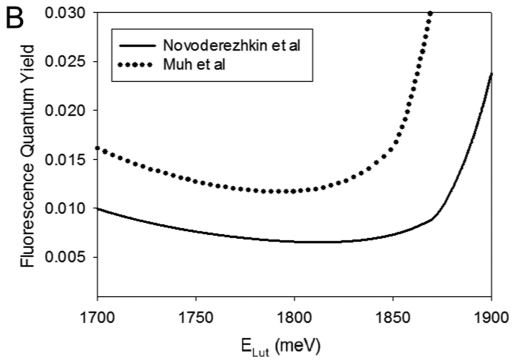

(b) FL quantum yield as a function of Lut 1 energy, taken from Ref. [6] *(1850 meV = 14920 cm^{-1}), the two curves correspond to chl site energies taken from the work of respective authors, see refs. in [6]*

Figure 4.4: Lutein 1 position and quenching ability

Let us test this mechanism and see if it can account for the blinking. The important parameters of the Lut are its site energy (by this we mean the vertical, Franck-Condon transition) and coupling to chlorophylls, mainly chl a612. We do not attempt to calculate these parameters from the first principles, but we treat them as free parameters and study their influence on the fluorescence quantum yield. In Fig. 4.5 we can see the dependence of the relative FL quantum yield on the Lut energy for fixed coupling 14 cm^{-1} and dependence on the coupling for fixed Lut energy 14500 cm^{-1}, which, due to large reorganization energy, corresponds to the zero-phonon line at 13900 cm^{-1} and thus agrees with experimental results of transient absorption by Polívka [24].

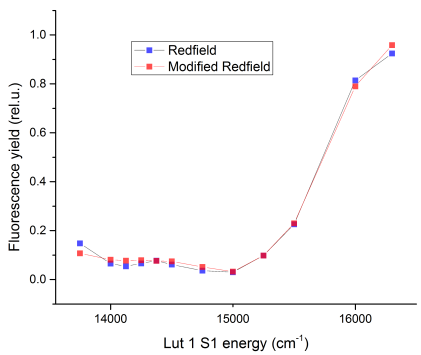

(a) S1 state energy

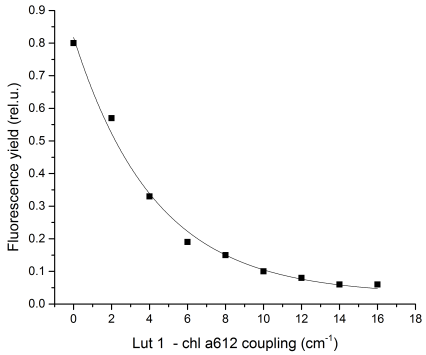

(b) coupling to chl a612

Figure 4.5: The Lut 1 parameters

Interestingly, the energy dependence agrees well with the one obtained by Ruban [6], see Fig. 4.4b. The quenching is really efficient when the Lut energy is below the red chlorophylls and the plateau means that it can act as a quencher even in energetically disordered systems, where the quenching effect will be stable for

different disorder realizations. From the dependence on coupling we can see that weak coupling is sufficient (this is given by the short lifetime of the Lut) and also that even a small change in the coupling can make a large difference in the fluorescence intensity. Based on this analysis we decide to use lutein S1 site energy 14500 cm^{-1} and coupling to chl 612 12 cm^{-1} in the quenched state and no coupling in the unquenched state.

4.5 Blinking

Here we apply the protein switching model described in section 3 to our data.

The parameters of the potentials are $\lambda_2/\lambda_1, \gamma_2/\gamma_1, x_0\sqrt{\lambda_1/k_BT}, y_0\sqrt{\gamma_1/k_BT}, U_0/k_BT$.

The parameters of the dynamics on the potentials are $D_{1y}\gamma_1/k_BT$, $D_{2y}\gamma_1/k_BT$.

The parameters of the tunneling are k_1, k_2, $\hbar\omega_0/\alpha k_BT$.

As discussed in section 3, we take $x_0 = 0$, $\lambda_2/\lambda_1 = 1$. Now we need the random switching with these parameters to control our excitonic model.

The switching simulation proceeds as follows:

We start at the potentials intersection point $y^{(0)}$: $U_1(y^{(0)}) = U_2(y^{(0)})$. This corresponds to the equilibrium condition described in 3, where the initial probability is a sharp peak localised at the intersection [3]. In each step the probability to jump is calculated using (3.8) as $p_{1\to2,2\to1} = \kappa_{1,2}(y)\Delta t$. If the system jumps, it changes the residing potential, if it does not it stays. After that the probability to go to the right/left is calculated using (3.15). According to that, the y coordinate is changed by $\pm a$. The parameters used for the simulation compared to the ones used originally by Valkunas *et al.* are given in Table 4.1. For this parameters the potentials intersection point is $y^{(0)} = 4.13$. The time step used is $\Delta t = 10$ ms.

parameter	Valkunas [31, pH 8]	This work
λ_1/λ_2	0.2	1.0
γ_1/γ_2	0.72	0.72
$x_0\sqrt{\lambda_1/k_BT}$	1.0	0.0
$y_0\sqrt{\gamma_1/k_BT}$	8.57	8.57
U_0/k_BT	1.5	1.5
k_1^{-1}	430 ms	200 ms
k_2^{-1}	4.8 ms	20 ms
$(D_1\gamma_1/k_BT)^{-1}$	3.8 s	7.7 s
$(D_2\gamma_1/k_BT)^{-1}$	1.4 s	2.7 s
$\hbar\omega_0/\alpha k_BT$	1.0	1.1

Table 4.1: RW model parameters

[3] This is physically strictly correct if the switching is at least partially photoinduced, i. e. when the system is in equilibrium before illuminated.

To connect this switching to our particular Lut quenching, we assume that the change of conformation somehow changes the Lut 1 - chla612 coupling. This makes sense since the coupling of Lut S1 state to the chlorophyll is of the Dexter type (as Lut S1 is dipole forbidden) and the coupling is thus extremely sensitive to distance between the two pigments [15]. The two different protein conformations would then result in the pigments being little closer/further, meaning different coupling. In our model we therefore simply assign to one surface zero coupling and to the second coupling of 12 cm^{-1}. We can check thus obtained on/off state distributions, see Fig. 4.6.

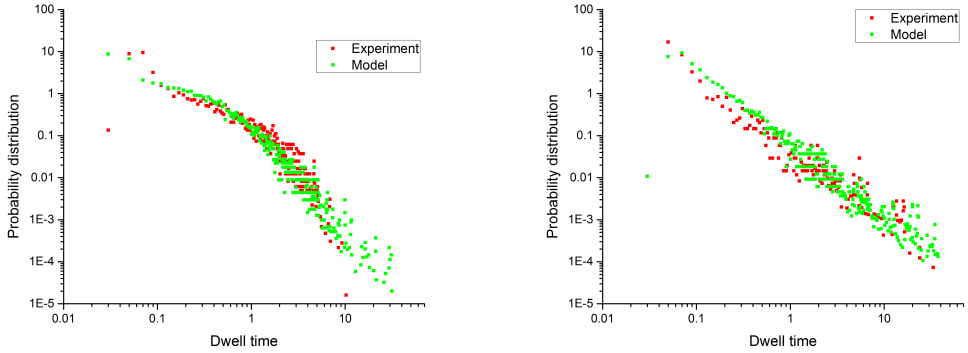

(a) On time

(b) Off time

Figure 4.6: Dwell times probability distribution

4.6 Single-molecule intensity traces

In Figs. 4.2 and 4.3 we see that the excitonic model describes well the spectral properties, in Fig. 4.5 we see that Lut 1 can work as a fluorescence quencher and Fig. 4.6 tells that the protein RW switching model can describe the blinking times statistics. All this means that the models can be used for LHCII and, most importantly, that they work with realistic parameters which correspond to the ones determined by other researchers. Now it is time to put the pieces of the puzzle together and try to simulate the blinking behaviour.

To this aim we continuously model the fluorescence of the LHCII complexes and output the intensity (and spectrum) every 10 ms, which corresponds to the experimental integration bins. Simultaneously we let the protein do the RW on its PES, and when it switches the coupling is changed. Also, to obtain more realistic traces, either the site energies or couplings can be slightly disordered after every jump (we used Gaussian disorder 0.3 cm^{-1} for couplings or 1 cm^{-1} for energies), resulting in slightly different energy levels, which agrees better visually with observations but can be omitted. For example of an intensity and spectral trace excerpt see Fig. B.1 in appendix B. For every realization of the disorder a 60 s trace is modelled and this is repeated for many realizations of the disorder, the resulting statistics are shown in Fig. 4.7. Total dwell times in Fig. 4.7a represent the overall amount of time spent in a given intensity level. From this we can see

the two-level character of the blinking and simultaneously also presence of some intermediate levels, which are caused by particular disorder realizations. Fig. 4.7b shows how often are the intensity levels visited per fixed amount of time. Comparing these two figures we can say that the low intensity levels are mostly either short or long lived, while for the bright ones the intermediate dwell times are also common. This, of course, corresponds to the on/off statistics used as an input.

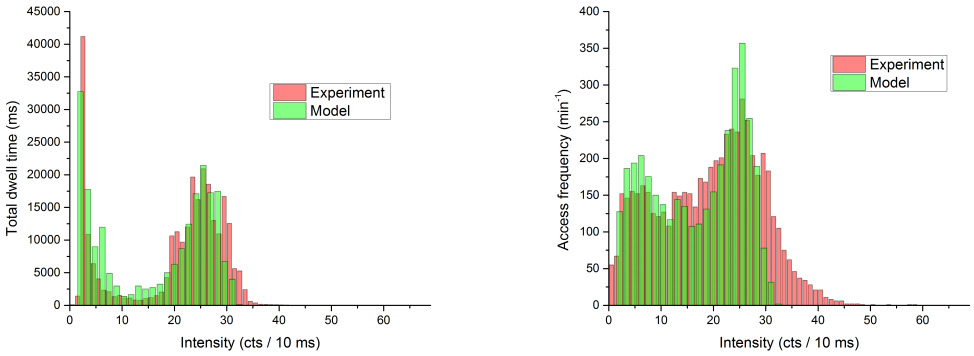

(a) Total dwell time distribution (b) Access Frequency distribution

Figure 4.7: Intensity traces statistics

Another way to quantify intensity traces statistics are the correlation functions [1]. We therefore calculate the normalized second-order (in intensity) correlation function

$$h^{(2)}(\tau) = \frac{\langle I(\tau)I(0)\rangle}{\langle I(0\rangle^2}. \tag{4.15}$$

Here $\langle\bullet\rangle$ means time average over the duration of the trace. The correlation function obtained from the model and experiment is compared in Fig. 4.8.

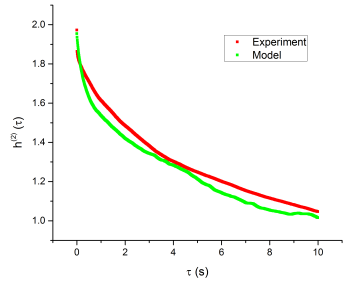

Figure 4.8: Intensity correlation function

Since our time resolution 10 ms is too low to observe antibunching corresponding to the optical transitions, we can see only the blinking-related part, namely the bunching expressed by $h^{(2)}(0) > 1$. The correlation function of the modelled

traces is somewhat lower but the shape corresponds well to the one obtained from experimental data. On the relatively small evaluated times range the correlation function is to a good degree exponential, which is expected from a Markovian 2-state kinetics [16], but some deviation in the short time is expected due to the non-Markovian property of the RW model used. The further use of correlation functions is one possible direction of our further research on stochastic trajectories sampling the disordered protein conformations.

Summary and discussion

The experimental part of this thesis focused on measuring the single-molecule spectra and traces of LHCII monomers. The outcome was highly similar to the previously observed LHCII trimers, including spectral shifts and fluorescence blinking. More than having much significance for interpreting the LHCII function in vivo on their own, the results thus serve as an invaluable basis for our theoretical calculations..

The first original theoretical work of this thesis focuses on derivation of the closed set of equations for the excitonic populations. The resulting form of the equations is highly intuitive, consisting of the internal system dynamics driven by the excitation light, where the only important property of the light is the overlap of its spectrum with the absorption spectrum of the system. What can be surprising is the relative low degree of approximation leading to this equations. First order perturbation theory in interaction with light is oftentimes used and can be experimentally easily realized. The secular approximation is used in most cases even when describing ultrafast dynamics and it has been shown that non-secular effects, if there are any, are mostly observed in the transient system dynamics, having little impact on steady state populations [7, 22]. Moreover, to authors knowledge there exists no experimental evidence for the importance of non-secular effects in biological systems, which are of interest here. Time-independent rates and slowly varying populations are also commonly used whenever the memory of the bath is short enough, resulting in the "coarse graining" of the time axis, which is no problem here since we are usually interested only in the steady state. Finally, inserting the light spectrum as a Fourier transform of the autocorrelation function can be also generalized by defining time-dependent spectrum [23, 8]. We note here that this inclusion of the light spectrum enables us, to our knowledge for the first time, to model population dynamics in for example photosynthetic complexes under realistic real-life conditions such as stationary AM1.5 sunlight illumination.

In the next part the derived equations are applied to LHCII monomers. As the excitonic properties of LHCII were already described elsewhere and are not of main interest here, we will not discuss their details. What is important is that the used excitonic model corresponds to previously published results and correctly describes the linear spectra. Since the fluorescence is given by the populations steady state which is calculated by our equations, we conclude that they are applicable in LHCII description.

Since the fluorescence blinking is a prominent feature of the intensity traces it is necessary to include some fluorescence quenching mechanism. Based on the recent research in elucidating NPQ mechanism in LHCII and connection between fluorescence quenching and energy dissipation we decided to try to implement energy transfer to Lut 1 as a blinking mechanism. Based on our calculations we were able to confirm the findings of Ruban *et al.* [6] that within a reasonable range of parameters Lut 1 can indeed act as an efficient quencher. Since our model

extends the previous treatment by including realistic excitation conditions and population transfer rates it is remarkable how similar is the fluorescence quenching dependence on the Lut 1 energy. Moreover, we were able to confirm that Lut 1 acts as an efficient quencher also under AM1.5 illumination (data not shown since the dependence is very similar). This may seem trivial but there definitely is a difference between arbitrarily chosen initial conditions such as even population of all pigments and realistic driving by light. In the same time we can see that the amount of quenching is very sensitive to the change of coupling of this Lut to the chlorophylls. Since the coupling itself is very sensitive to the distance between the pigments, it provides possible link to the protein conformation change working as a switching mechanism.

The switching itself is successfully governed by discrete random walk in a potential with a possibility of quantum tunneling between two states. The generation of stochastic trajectories enables us to to simulate individual traces. Remarkable is that although we, in contrast to original treatment by Valkunas *et al.* [31], did not include the resetting after switching and simulated monomers instead of trimers, were able to reproduce the dwell time distributions with very similar potential parameters. Moreover, when using this 2-level switching model to control the change of chl a612-lut 620 coupling, we are able to reproduce the experimentally obtained blinking statistics. Although far from being exclusive in any way, our argument strongly supports the notion of the protein acting as a conformational switch regulating the amount of quenching in the system.

The agreement between the theory and experiment also serves as a good demonstration of the scope of our equations. They provide a description for controlling the energy transfer in the system by modulating the parameters of the excitonic model. We are thus able to simulate the single-molecule intensity and spectral traces on the experimental timescale. Since the modelled trace analysis agrees with experimental data, we can conclude that the models can indeed be connected in the way we demonstrated and thus form one, consistent picture of LHCII function.

Outlook

From the experimental side more work in the direction of elucidating the relation between the fluorescence blinking and the protein conformational change is needed. One possibility is to try to stabilize the protein structure. As it was recently demonstrated by Ilioaia *et al.*, LHCII can be fixed in either quenched or unquenched state by cross-linking with glutaraldehyde (GA). Single-molecule study of GA treated LHCII could therefore be of interest. Another possible direction is to try and change the parameters which play role in the protein switching, such as temperature. Finally, connection to the results of another experiment sensitive to the conformational change, such as circular dichroism or Raman spectroscopy, could be made.

From the theoretical side there are several options for extending our work. As our approach to calculating single-molecule signals is general, it could be applied on SMS of other (biological) systems, where the approximations used here also work. The particular switching mechanism controlling the excitonic model would be different, but the equations remain the same. Moreover, because our equations can easily be used under real-life illumination conditions, i. e. weak sunlight, they can be employed to test the mechanisms proposed elsewhere.

There is still room for further work on LHCII as well. We are aware of the remaining phenomenological nature of our connection of the 2-level switching model with the excitonic model. Improvements in the direction of introducing more parameters with particular physical meaning, for example relation to the actual PES shape, are needed and will be subject to further study. One such possibility is to relate some projection of the generalized coordinate used for switching to the distance between the chl a612 and lut 620. Also recent experimental observations indicate possible presence of more relevant timescales in the intensity traces suggesting the inadequacy of a 2-level model with one reaction coordinate. Another option in reducing the phenomenology is letting the pigments sample their disorder in some controlled way, e. g. by trajectories of a random walk again in some potential. This would preserve the Gaussian distribution of the site energies and, in the same time, allow for simulation of realistic spectral diffusion. Finally, although some connection between the fluorescence blinking and NPQ was already shown by Krüger *et al.*, their exact relation is yet to be elucidated. To this goal parameters which determine NPQ conditions such as pH and also the influence of the membrane potential should be included in the model.

From the extent of possibilities outlined above it is clear that the work presented in this thesis is by no means the final solution to any problem. It much more resembles an important piece of puzzle. A piece which connects several other pieces together, hopefully bringing us one step closer to seeing the whole picture.

A. Excitonic model - parameters

In this appendix we list the parameters of the excitonic model. The system Hamiltonian including Lutein 1 in the quenched mode (coupled to chl a612) is presented in Table A.1. The bold, diagonal values are the site energies (pigment vertical electronic transitions), the off-diagonal elements are the couplings calculated in the dipole-dipole approximation (and, for the lutein, taken from [6]).

	602	603	610	611	612	608	609	601	613	614	604	605	606	607	Lut 1
602	**15160**	35.95	-11.76	9.55	16.14	-6.18	-19.59	52.43	-5.56	0.94	6.45	-0.73	5.69	7.32	0.00
603	35.95	**15283**	13.18	-2.52	-0.91	7.81	98.01	-6.20	1.86	-6.79	-3.74	1.24	-9.28	1.53	0.00
610	-11.76	13.18	**15073**	-25.77	24.62	62.23	4.37	-6.08	7.33	-1.65	-4.28	1.61	-3.38	-0.13	-0.80
611	9.55	-2.52	-25.77	**15115**	137.91	4.43	4.52	26.73	-6.09	4.41	-3.96	1.40	-2.62	-2.91	0.00
612	16.14	-0.91	24.62	137.91	**15097**	-1.10	-2.80	9.36	-0.68	-0.01	5.06	-2.98	3.25	3.21	12.00
608	-6.18	7.81	62.23	4.43	-1.10	**15763**	38.99	2.93	-1.98	1.37	-2.88	-5.36	-5.22	-4.82	1.60
609	-19.59	98.01	4.37	4.52	-2.80	38.99	**15721**	4.03	-2.95	2.40	-7.48	-0.84	0.54	-12.32	0.00
601	52.43	-6.20	-6.08	26.73	9.36	2.93	4.03	**15890**	-10.82	3.56	-2.60	0.81	-1.99	-2.62	0.00
613	-5.56	1.86	7.33	-6.09	-0.68	-1.98	-2.95	-10.82	**15175**	-53.87	1.96	-1.46	1.39	2.05	0.00
614	0.94	-6.79	-1.65	4.41	-0.01	1.37	2.40	3.56	-53.87	**15264**	-3.48	0.40	-2.25	-3.41	0.00
604	6.45	-3.74	-4.28	-3.96	5.06	-2.88	-7.48	-2.60	1.96	-3.48	**15460**	3.61	112.27	37.07	0.00
605	-0.73	1.24	1.61	1.40	-2.98	-5.36	-0.84	0.81	-1.46	0.40	3.61	**15679**	33.04	-4.51	0.00
606	5.69	-9.28	-3.38	-2.62	3.25	-5.22	0.54	-1.99	1.39	-2.25	112.27	33.04	**15851**	60.96	0.00
607	7.32	1.53	-0.13	-2.91	3.21	-4.82	-12.32	-2.62	2.05	-3.41	37.07	-4.51	60.96	**15712**	0.00
Lut 1	0.00	0.00	-0.80	0.00	12.00	1.60	0.00	0.00	0.00	0.00	0.00	0.00	0.00	0.00	**14500**

Table A.1: LHCII Hamiltonian including Lut 1
all values are in cm^{-1}

The parameters of the spectral density can be found in Ref. [19], the coupling to the phonons was taken $\nu_a = 1$ for chl a and $\nu_b = 1.2$ for chl b. The spectral density with the dominant high-frequency modes is in Fig. A.1.

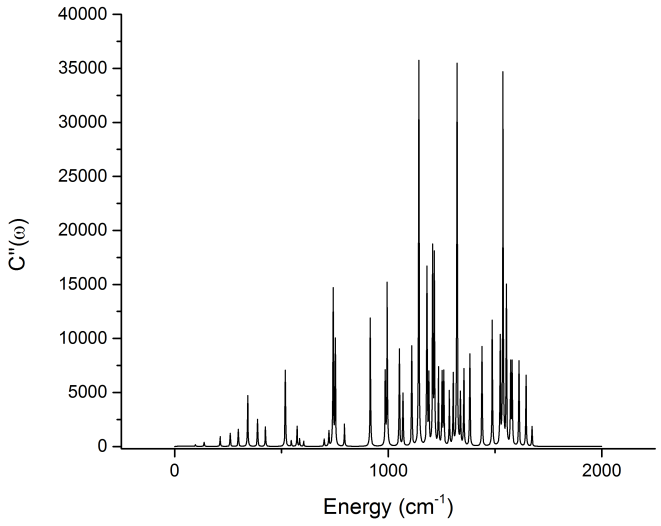

Figure A.1: Spectral density of the bath

B. Simulated traces

In Fig. B.1 we present examples of the generated traces described in section 4.6. When visually comparing with experimentally obtained traces it is important to note the absence of the noise.

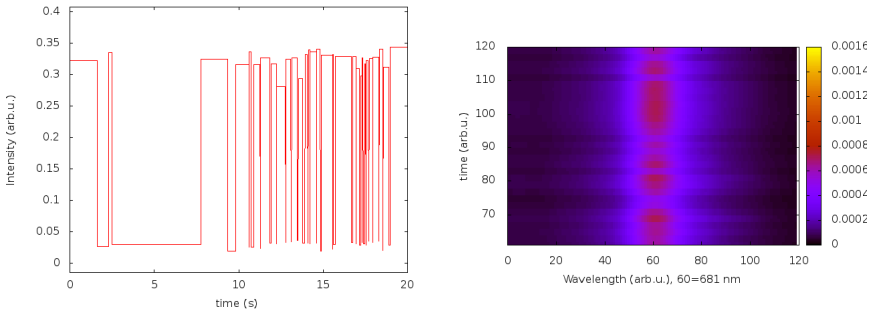

(a) Intensity trace (b) Spectral trace

Figure B.1: Simulated traces example

Bibliography

[1] Barkai, E., Brown, F. L. H., Orrit, M., and Yang, H., editors. *Theory and Evaluation of Single-Molecule Signals*. World Scientific 2008.

[2] Blankenship, R. E. *Molecular Mechanisms of Photosynthesis*. Blackwell Science 2002.

[3] Brumer, P. and Shapiro, M. Molecular response in one-photon absorption via natural thermal light vs. pulsed laser excitation. *Proc. Natl. Acad. Sci. U. S. A.* 2012, *109*, 19575.

[4] Chmeliov, J., Valkunas, L., Krüger, T. P. J., Ilioaia, C., and van Grondelle, R. Fluorescence blinking of single major light-harvesting complexes. *New Journal of Physics* 2013, *15*, 085007.

[5] Drop, B., Webber-Birungi, M., Yadav, S. K. N., Filipowicz-Szymanska, A., Fusetti, F., Bokema, E. J., and Croce, R. Light-harvesting complex ii (lhcii) and it supramolecular orgaization in chlamydomonas reinhardtii. *Biochimica et Biophysica Acta* 2014, *1837*, 63.

[6] Duffy, C. D. P., Chmeliov, J., Macernis, M., Sulskus, J., Valkunas, L., and Ruban, A. V. Modeling of fluorescence quenching by lutein in the plant light-harvesting complex lhcii. *J. Phys. Chem. B* 2013, *117*, 10974.

[7] Jesenko, S. and Žnidarič, M. Excitation energy transfer efficiency: Equivalence of transient and stationary setting and the absence of non-markovian effects. *Journal of Chemical Physics* 2013, *138*, 174103.

[8] Jiang, X.-P. and Brumer, P. Creation and dynamics of molecular states prepared with coherent vs partially coherent pulsed light. *J. Chem. Phys.* 1991, *94*, 5833.

[9] Krüger, T. P. J., Ilioaia, C., and van Grondelle, R. Fluorescence intermittency from the main plant light-harvesting complex: Resolving shifts between intensity levels. *Journal of Physical Chemistry B* 2011, *115*, 5071.

[10] Krüger, T. P. J. *From Disorder to Order: The functional flexibility of single plant light-harvesting complexess*. PhD thesis Vrije Universiteit Amsterdam 2011.

[11] Krüger, T. P. J., Ilioaia, C., Valkunas, L., and van Grondelle, R. Fluorescence Intermittency from the Main Plant Light-Harvesting Complex: Sensitivity to the Local Environment. *J. Phys. Chem. B* 2011, *115*, 5083.

[12] Krüger, T. P. J., Novoderezhkin, V., Ilioaia, C., and van Grondelle, R. Fluorescence spectral dynamics of single lhcii trimers. *Biophys. J.* 2010, *98*, 3093.

[13] Liu, Z., Yan, H., Wang, K., Kuang, T., Zhang, J., Gui, L., An, X., and Chang, W. Crystal structure of spinach major light-harvesting complex at 2.72 å resolution. *Nature* 2004, *428*, 287.

[14] Mančal, T. and Valkunas, L. Exciton dynamics in photosynthetic complexes: excitation by coherent and incoherent light. *New Journal of Physics* 2010, *12*, 065044.

[15] May, V. and Kühn, O. *Charge and Energy Transfer Dynamics in Molecular Systems*. Wiley-VCH 2011.

[16] Moerner, W. and Fromm, D. P. Methods of single-molecule fluorescence spectroscopy and microscopy. *Review of Scientific Instruments* 2003, *74*, 3597.

[17] Mukamel, S. *Principles of nonlinear spectroscopy*. Oxford University Press Oxford 1995.

[18] Novoderezhkin, V., Marin, A., and van Grondelle, R. Intra- and inter-monomeric ttransfer in the light harvesting lhcii complex: the redfield-förster picture. *Physical Chemistry Chemical Physics* 2011, *13*, 17093.

[19] Novoderezhkin, V. I., Palacios, M. A., van Amerongen, H., and van Grondelle, R. Energy-transfer dynamics in the lhcii complex of higher plants: Modified redfield approach. *J. Phys. Chem. B* 2004, *108*, 10363.

[20] Novoderezhkin, V. I., Palacios, M. A., van Amerongen, H., and van Grondelle, R. Excitation dynamics in the lhcii complex of higher plants: Modeling based on the 2.72 å crystal structure. *J. Phys. Chem. B* 2005, *109*, 10493.

[21] Novoderezhkin, V. I. and van Grondelle, R. Physical origins and models of energy transfer in photosynthetic light-harvesting. *Physical Chemistry Chemical Physics* 2010, *12*, 7352.

[22] Olšina, J. and Mančal, T. Electronic coherence dephasing in excitonic molecular complexes: Role of markov and secular approximations. *J. Mol. Model.* 2010, *16*, 1765.

[23] Page, C. H. Instantaneous power spectra. *J. Appl. Phys.* 1952, *23*, 103.

[24] Polívka, T., Zigmantas, D., and Sundström, V. Carotenoid s1 state in a recombinant light-harvesting complex of photosystem ii. *Biochemistry* 2002, *41*, 439.

[25] Richter, M. F., Baier, J., Cogdell, R. J., Köhler, J., and Oellerih, S. Single-molecule spectroscopic characterization of light-harvesting 2 complexes reconstituted into model membranes. *Biophysical Journal* 2007, *93*, 183.

[26] Ruban, A. V., Berera, R., Ilioaia, C.and van Stokkum, I. H. M., Kennis, J. T. M., Pascal, A. A., van Amerongen, H., Robert, B., Horton, P., and van Grondelle, R. Identification of a mechanism of photoprotective energy dissipation in higher plants. *Nat. Lett.* 2007, *450*, 575.

[27] Ruban, A. V., Johnson, M. P., and Duffy. The photoprotective molecular switch in the photosystem ii antenna. *Biochimica* 2012, *1817*, 167.

[28] Schlau-Cohen, G. S., Calhoun, T. R., Ginsberg, N. S., Read, E. L., Ballotari, M., Bassi, R., van Grondelle, R., and Fleming, G. R. Pathways of energy flow

in lhcii from two-dimensional electronic spectroscopy. *Journal of Physical Chemistry B* 2009, *113*, 15352.

[29] Tietz, C., Jelezko, F., Gerken, U., Schuler, S., Schubert, A., Rogl, H., and Wrachtrup, J. Single molecule spectroscopy on the light-harvesting complex ii of higher plants. *Biophysical Journal* 2001, *81*, 556.

[30] Valkunas, L., Abramavicius, D., and Mančal, T. *Molecular Excitation Dynamics and Relaxation.* Wiley-VCH 2013.

[31] Valkunas, L., Chmeliov, J., Krüger, T. P. J., Ilioaia, C., and van Grondelle, R. How photosynthetic proteins switch. *J. Phys. Chem. Lett.* 2012, *3*, 2779.

[32] van Amerongen, H., van Grondelle, R., and Valkunas, L. *Photosynthetic Excitons.* World Scientific 2000.

[33] van Kampen, N. G. *Stochastic processes in physics and chemistry.* North Holland 1992.

[34] Wahadoszamen, M., Berera, R., Ara, A. M., Romero, E., and van Grondelle, R. Identification of two emitting sites in the dissipative state of the major light harvesting antenna. *Physical Chemistry Chemical Physics* 2012, *14*, 759.